Published in final edited form as:
J Chem Neuroanat. 2009 January ; 37(1): 18–32. doi:10.1016/j.jchemneu.2008.08.002.

Rapid Morphological Brain Abnormalities during Acute Methamphetamine Intoxication in the Rat. An Experimental study using Light and Electron Microscopy

Hari S. Sharma[a,b,*] and **Eugene A. Kiyatkin**[b]

a *Laboratory of Cerebrovascular Research, Department of Surgical Sciences, University Hospital, Uppsala University, SE-751 85 Uppsala, Sweden*

b *Behavioral Neuroscience Branch, National Institute on Drug Abuse–Intramural Research Program, NIH, 5500 Nathan Shock Drive, Baltimore, MD 21224, USA*

Abstract

This study describes morphological abnormalities of brain cells during acute methamphetamine (METH) intoxication in the rat and demonstrates the role of hyperthermia, disruption of the blood-brain barrier (BBB) and edema in their development. Rats with chronically implanted brain, muscle and skin temperature probes and an intravenous (iv) catheter were exposed to METH (9 mg/kg) at standard (23°C) and warm (29°C) ambient temperatures, allowing for the observation of hyperthermia ranging from mild to pathological levels (38–42°C). When brain temperature peaked or reached a level suggestive of possible lethality (>41.5°C), rats were injected with Evans blue (EB), rapidly anesthetized, perfused, and their brains were taken for further analyses. Four brain areas (cortex, hippocampus, thalamus and hypothalamus) were analyzed for EB extravasation, water and electrolyte (Na^+, K^+, Cl^-) contents, immunostained for albumin and glial fibrillary acidic protein, and examined for neuronal, glial and axonal alterations using standard light and electron microscopy. These examinations revealed profound abnormalities in neuronal, glial, and endothelial cells, which were stronger with METH administered at 29°C than 23°C and tightly correlated with brain and body hyperthermia. These changes had some structural specificity, but in each structure they tightly correlated with increases in EB levels, the numbers of albumin-positive cells, and water and ion contents, suggesting leakage of the BBB, acutely developing brain edema, and serious shifts in brain ion homeostasis as leading factors underlying brain abnormalities. While most of these acute structural and functional abnormalities appear to be reversible, they could trigger subsequent cellular alterations in the brain and accelerate neurodegeneration—the most dangerous complication of chronic amphetamine-like drug abuse.

Keywords

methamphetamine; blood-brain barrier; brain edema; brain pathology; glial cells; neuronal damage; myelin vesiculation; ultrastructural changes; endothelial cells

Correspondence should be addressed to Hari S. Sharma, PhD, Dr. Med. Sci Frödingsgatan 12: 28, SE-75421 Uppsala, Sweden, Phone & Fax: +46-18-243899, e-mail: Sharma@surgsci.uu.se.

It is known that methamphetamine (METH) is a neurotoxic addictive drug and its repeated use could result in degenerative brain changes primarily involving terminals of dopamine and serotonin neurons (Ricaurte et al., 1980; Seiden and Sabol, 1996). While irreversible damage of neural and non-neural brain cells is the obvious cause of neurological and psychiatric abnormalities in chronic METH users, acute METH intoxication may result in serious decompensation of physiological functions with possible lethality. In contrast to the multiple factors contributing to chronic METH neurotoxicity (oxidative stress with production of oxygen and nitrogen reactive species, aberrant dopamine and glutamate transmission, excitotoxicity, mitochondrial dysfunctions, apoptosis, astroglial and microglial activations, etc. see Cadet et al., 2005, 2007; Thomas et al., 2004; Yamamoto and Bankson, 2005 for review), the mechanisms underlying life-threatening effects of acute METH intoxication remain less clear.

It is known that METH induces metabolic activation (Estler, 1975; Makisumi et al., 1998) associated with body hyperthermia (Alberts and Sonsalla, 1995; Kalant and Kalant, 1975; Miller and O'Callaghan, 1994; Sandoval et al., 2000). METH also induces brain hyperthermia (Brown et al., 2003), with stronger and more rapid temperature increases than in peripheral sites. Confirming previous work on the potentiating effects of ambient temperature on METH toxicity (Ali et al., 1996; Bowyer et al., 1994), we showed that even a slight increase in ambient temperature (29°C) strongly potentiates METH-induced hyperthermia, resulting in lethality in most rats at a fraction of LD_{50} doses (Brown and Kiyatkin, 2005). Since brain cells are exceptionally sensitive to high temperature (see Sharma, 2006 and Kiyatkin, 2005 for review), METH-induced hyperthermia might be an important contributor to pathological perturbations in brain structure and functions. Along with possible direct effects on brain cells, hyperthermia could affect the permeability of the blood-brain barrier (BBB), thus allowing serum proteins, potentially neurotoxic substances, and water to enter the cerebral microenvironment from the peripheral circulation and resulting in serious alterations of ionic brain homeostasis, development of brain edema and possible damage of brain cells (Sharma and Hoopes, 2003; Sharma, 2006). Confirming and extending previous observations (Bower and Ali, 2006; Sharma and Ali, 2006), we recently showed that METH induces robust and widespread BBB leakage as demonstrated by Evans Blue (EB) diffusion in brain tissue and albumin immunoreactivity; these changes tightly correlated with the intensity of brain hyperthermia (Kiyatkin et al., 2007).

The present study is focused on morphological brain abnormalities developing during acute METH intoxication and basic pathophysiological mechanisms that are involved in their development. All rats received METH at the same, moderate dose (9 mg/kg, sc or ~1/5 LD_{50}; Derlet et al., 1990) at either standard (23°C) or warm (29°C) ambient temperatures, allowing for observation of brain hyperthermia ranging from mild to extreme (37.5–42.0°C). The brains were taken for further analyses when temperatures peaked or reached clearly pathological levels (>41.5°C) suggesting a possible lethality. To establish common features and structural specificity, measurements were made in the cortex, hippocampus, thalamus and hypothalamus as well as other specific brain areas of interest. Along with morphological examination of neuronal, glial and axonal alterations using standard light and electron microscopy, individual brain areas were also analyzed for EB extravasation, water and electrolyte (Na^+, K^+, Cl^-) contents, and immunostained for albumin and glial fibrillary acidic protein (GFAP). The neuropathological changes were evaluated to define structural and cellular specificity of neural abnormalities in relation to brain and body hyperthermia, BBB leakage, and brain edema.

Materials and Methods

Animals and Surgery

Experiments were carried out on 21 male Long-Evans rats (420±40 g) supplied by Charles River Laboratories (Greensboro, NC). All animals were housed individually under standard laboratory conditions (21±1°C; ambient temperature; 12-hr light cycle beginning at 07:00), with food and water provided *ad libitum*. Protocols were performed in compliance with the Guide for the Care and Use of Laboratory Animals (NIH, Publication 865-23) and were approved by the NIDA-IRP Animal Care and Use Committee. Maximal care was taken to both minimize the number of animals used and their suffering.

All animals were chronically implanted with three thermocouple electrodes as previously described (Kiyatkin et al., 2007). Animals were anesthetized with Equithesin (3.3 ml/kg i.p.; total volume containing sodium pentobarbital 32.5 mg/kg and chloral hydrate 145 mg/kg) and mounted in a stereotaxic apparatus. Burr holes were drilled through the skull over the nucleus accumbens (NAcc) shell (1.2 mm anterior to bregma, 0.9 mm lateral to bregma) using the coordinates of Paxinos and Watson (1998). The *dura mater* was retracted and a thermocouple probe was slowly lowered into the desired target depth (7.4 mm). Second and third thermocouple probes were implanted, respectively, in deep temporal muscle (*musculus temporalis*) and subcutaneously along the nasal ridge with the tip approximately 15 mm from bregma. These two locations were important to examine the contributions of alterations in vascular tone and arterial blood temperature to drug-induced brain hyperthermia. All three probes were secured with dental cement to three stainless steel screws threaded into the skull. During the same surgery, each animal was also implanted with a jugular intravenous (iv) polythene catheter. Rats were allowed three days recovery and two days of habituation (6–8 hrs) before the start of testing.

Experimental Protocol

All tests occurred inside a light- and sound-attenuated Plexiglas chambers (32×32×32 cm) equipped with four infrared motion detectors (Med Associates, Burlington, VT, USA). Rats were brought to the testing chamber and attached via a flexible cord and electrical commutator to thermal recording hardware (Thermes 16, Physitemp, Clifton, NJ, USA). A catheter extension was also attached to the internal catheter, thereby allowing a remote, unsignalled iv injection. The catheter was filled with 2% solution of Evans Blue (EB; Sigma, USA; dissolved in saline), which was injected at a specified time following sc injections (see below). Temperatures were recorded with a time resolution of 10 s and movement was recorded as the number of infrared beam breaks per 1 min.

The animals were divided into three groups: (a) control at 23°C; (b) METH at 23°C; and (c) METH at 29°C. After 3 hrs habituation to the testing chamber, control rats (n=5) received a single subcutaneous (sc) saline injection (0.3 ml), while rats from the other two groups (n=8 each) received a single sc METH injection (in 0.3 ml saline) either at 23 or 29°C ambient temperatures. At a specified time following drug or saline injection, EB was administered into the jugular vein catheter (3 ml/kg over 60 s) and the dye was allowed to circulate for 5 min. At the end of 5 min, the animals were rapidly anesthetized with iv Equithesin (0.8 ml over 30 s), and taken for brain perfusion (see below). Animals were perfused with cold Somogyi fixative (0.4 % paraformaldehyde solution containing 0.5 % glutaraldehyde and 2.5 % picric acid in phosphate buffered saline, PBS, 0.1 M, pH 7.4) at the rate of 20 ml/min for 10 min (Sharma et al., 1992). The intravascular blood was washed-out before fixation by 0.1 M PBS or saline (20 ml/min for 5 min). The perfusion pressure was maintained at 100 torr during these procedures. The animals were wrapped in aluminum foil and kept in a refrigerator at 4°C

overnight. On the next day, the brain was removed and kept in the same fixative at 4°C for ~21 days.

While all control animals were injected with EB 120 min after saline administration, the moment of dye injection in METH-treated animals was determined by observing peak temperature or extremely high temperature (>41.5°C). In a METH-23°C group, this time varied from 66 to 94 min and in a METH-29°C group, it varied from 26 to 79 min.

Morphological Observations and Measurements

Measurement of Brain Edema—The tissue water content was calculated from the differences between dry and wet weights of the sample (Sharma and Cervós-Navarro, 1990) and ion content (Na^+, K^+ and Cl^-) was measured from the dry weight of the samples as described earlier (Joo et al., 1976; Sharma, 2004). In brief, the cortical areas from the occipital and cingulate cortices, hippocampus, thalamus and hypothalamus were dissected out from one half of coronal brain sections, weighed separately and placed in an oven maintained at 90°C for 72 h to obtain dry weight of the samples. After obtaining the dry weight, the tissues samples were processed for determination of Na^+, K^+ and Cl^- using atomic absorption spectrophotometry.

Measurement of BBB permeability—The integrity of the BBB function was evaluated based on leakage of EB on the dorsal and ventral surfaces of the brain as well as staining of the brain areas in three different coronal slices (measured from bregma), corresponding to forebrain (+0.10 to +0.45 mm), diencephalon (−3.25 to −3.90 mm) and midbrain (−4.20 to −4.60 mm). After visualization of the blue dye staining, parietal and cingulate cortices, hippocampus, thalamus, and hypothalamus were dissected out of the coronal section passing through the diencephalon, and the dye content was measured colorimetrically as described in detail earlier (see Kiyatkin et al., 2007; Sharma and Sjöquist, 2002).

Immunohistochemistry—Thin pieces of coronal sections from the diencephalon were used for immunostaining for albumin and glial fibrillary acidic protein (GFAP).

Immunohistochemistry for albumin was performed on vibratome (60 μm thick) sections using a sheep polyclonal anti-rat albumin antibody (Sigma, USA) and the streptavidin-HRP-biotin technique as described previously (Sharma et al., 1992; 1995). Albumin-positive cells were counted in anatomically defined brain regions, e.g., the cortex, hippocampus, thalamus and hypothalamus. GFAP immunostaining was performed using a commercial protocol, using 3–5 μm coronial brain sections obtained from the diencephalon. GFAP-positive cells were counted separately in the cortex, hippocampus, thalamus and hypothalamus.

The myelin basic protein (MBP) immunostaining was examined on paraffin-embedded 3 μm thick brain sections. In brief, brain sections were incubated with monoclonal myelin basic protein (MBP) antibody (1:500) at 4°C overnight. The immunostaining was developed using standard commercial procedures using a peroxidase-antiperoxidase reaction and counterstained with eosin as described in detail earlier (Sharma et al., 1993).

To identify myelinated and unmyelinated nerve fibers, Luxol Fast Blue staining was performed according to commercial histological protocol. Some sections were also counterstained with eosin, while most sections were examined only using Luxol Fast Blue staining.

Structural alterations—Structural changes were examined in identical brain regions, corresponding to the cortex, hippocampus, thalamus and hypothalamus at light and electron microscopy using standard procedures as described earlier (Sharma et al., 1993, 1995). For light microscopy, 3-μm paraffin sections were stained with Haematoxylin and Eosin or Nissl.

The criteria for abnormal cells were the presence of one or more of the following characteristics: vacuolated cytoplasm, dark stained and condensed cell nucleus and cell cytoplasm, no nucleus or no clear nucleolus, shrunken or swollen shape. The numbers of distorted cells having one or all the above parameters in the defined anatomical regions were counted manually in a blind fashion. Although all these indices suggest structural abnormalities, their presence does not mean that that the cell is irreversibly damaged. Significant time is necessary for the damaged cells to become dead and be verified as dead, using special histochemical techniques (see Bowyer and Ali, 2006).

Small pieces from the cerebral cortex, hippocampus, thalamus and hypothalamus were cut, post fixed in osmium tetraoxide and embedded in Epon for transmission electron microscopy (TEM) (see Sharma et al., 1993, 1995). The TEM analysis was done in selected groups of rats from METH-23°C (n=5), METH-29°C (n=5) that showed the highest levels of hyperthermia as well as in three control rats. About 1-μm thick, plastic embedded (Epon 812) tissue sections were cut for high-resolution light microscopy and stained with Tolouidine blue. The specific portions of the tissue comprising small microvessels and the neuropil were trimmed out and ultra-thin sections were cut using an LKB ultramicrotome (Stockholm, Sweden) using a diamond knife. These ultra-thin sections were collected on one hole copper grid and counterstained with lead citrate and uranyl acetate and examined under a Phillips 400 transmission electron microscope. The microvessels from identical brain structures regions were analyzed for perivascular edema, distortion of the endothelial cells and vacuolation of the neuropil. In addition, we also examined at the ultrastructural level myelin damage and distortion of nerve cells and glial cells.

Data Analyses

Temperature and movement data were analyzed with 2-min time bins and presented as both absolute and relative changes with respect to the moment of drug administration. Functional and morphological parameters were analyzed both in groups (control, METH-23°C and METH-29°C) and individually to define their relationships. ANOVA with repeated measures, followed by post-hoc Fisher tests, was used for statistical evaluation of drug-induced changes in temperature and movement. Student's t-test was used for comparisons of between-site differences in temperature and locomotion. Correlative and regression analyses were used to assess the relationships between temperatures and other brain parameters.

Results

As shown in Fig. 1, METH induced NAcc and muscle hyperthermia in both animal groups (A). In each group, basal temperatures in the NAcc were about 0.5–0.8°C higher than in the muscle, and NAcc temperature increased more rapidly and stronger than in muscle. In contrast, temperature in the skin, which was ~0.8°C lower than in muscle, rapidly decreased after METH injection, reflecting acute vasoconstriction and diminished heat loss to the external environment. Then, skin temperature also slowly increased, following brain and muscle temperatures. At the moment when brains were taken, skin temperature in the METH-23°C group was equal to control, but significantly higher than control in the METH-29°C group.

The METH-induced NAcc temperature increase highly varied in both groups, but was statistically greater at 29°C (range 40.26 to 41.91°C; mean 41.37±0.22°C) than 23°C (range 37.52°C to 40.13°C; mean 38.92±0.34°C). Between-group differences were also evident in muscle temperatures, but the increase in this case was relatively weaker than in the brain (1.99 vs. 2.31°C and 3.68 vs. 4.13°C for METH-23 and METH-29°C, respectively). Importantly, the degree of hyperthermia was not related to the time of drug exposure. In the METH-23°C group, NAcc temperatures peaked from 66 to 94 min after drug injection (mean 88.88±3.96 min). This time varied from 26 to 79 min in the METH-29°C group and its mean value (58.13

±5.82 min) was significantly shorter than in the METH-23°C group. Despite differences in absolute values, NAcc and muscle temperature evaluated at the final points of recording were tightly correlated (see Fig. 1B).

Alterations in the BBB permeability

As shown in Table 1, each brain structure differed in basal EB leakage in control intact brains. The cortex showed minimal EB content, followed by the hippocampus, thalamus and hypothalamus, which both had a higher EB content than cortical tissue. In animals administered with METH at 23°C, all structures had significantly higher EB content compared to control. The increase was stronger in the cortex (+133 %) and hippocampus (+134 %) and weaker in the hypothalamus (+71%) and thalamus (+66 %). Animals administered with METH at 29°C showed significantly higher increases in EB in all the regions. In this case, the increase was greatest in the cortex (+390%), followed by the hippocampus (+261 %), hypothalamus (+109 %) and thalamus (+107 %).

Immunohistochemistry for albumin showed a close correspondence with EB levels in different structures. As shown in a representative example of immunostained cortical tissue (see Fig. 2a), the leakage of albumin in the neuropil was clearly larger than control in animals that received METH, and was clearly more prominent in animals that were exposed to the drug at 29°C than 23°C. Quantitative analysis of albumin-positive cells (Table 2) showed a significant increase in each brain structure, which was again maximal in the cortex and hippocampus and lower in the thalamus and hypothalamus. The number of albumin-positive cells was significantly higher when METH was administered at 29°C than 23°C. Here again, the cerebral cortex and hippocampus showed the strongest increase (29.25±1.60 immunopositive cells/section or 49-fold vs. control and 26.88±1.13 cells/section or 24-fold vs. control) followed by the thalamus (17.88±1.13) and hypothalamus (15.00±0.78).

Relationships between brain temperature and permeability of the BBB

As shown in Fig. 3, both EB levels (top) and counts of albumin-positive cells (bottom) were tightly related to brain and body hyperthermia in all analyzed brain structure. Despite differences in regression lines, correlation was tight for both EB and albumin staining, and equally strong with respect to brain and muscle temperatures. Therefore, BBB leakage is strongly temperature-dependent.

Alterations in water and ion content

In agreement with the previous findings on regional differences in brain water content (Rapoport, 1976), we found that the hippocampus has higher water content than cortex and the underlying thalamus and hypothalamus in control conditions (Table 1). METH administered at 23°C induced a strong increase in water content in each structure, but as a relative change the increase was similar in the cortex, hippocampus and thalamus (1.3–1.4%) but weaker in the hypothalamus (0.9%). The increase was dramatically larger in the METH-29°C group, but the pattern did not differ significantly in various structures. Thus, the cortex and hypothalamus exhibited about 2.9 and 3.1% increase over control values, while the thalamus and hypothalamus showed a 2.8 and 2.6% elevations.

METH treatment also resulted in a general increase in Na^+, K^+ and Cl^- contents in various brain areas, and this increase was stronger when METH was used at 29°C than 23°C (Table 1). Levels of each ion varied in control condition, with Na^+ being the most prevalent and Cl^- being the least. Among structures, the Na^+, K^+ and Cl^- contents in control were highest in the hippocampus, followed by cortex, hypothalamus and thalamus. With respect to Na^+, the increase seen in the METH-23°C group vs. control was significant and almost identical in each structure (+30–36 mM/kg). With respect to K^+ and Cl^-, the increase was structure-specific,

with no changes of K^+ in the cortex and hippocampus and no changes in Cl^- in the hippocampus and hypothalamus in the METH-23°C group. In fact, cortical K^+ levels were even lower than in control. However, the levels of all ions were significantly higher in METH-29°C vs. control. The increase in Na^+ was most pronounced, with greatest change in the hypothalamus (+72 mM/kg) and thalamus (+62 mM/kg). These two structures also showed largest increases in Cl^- (32 nM and 33 nM, respectively), although the increases in this ion were qualitatively lower than those for Na^+. The increases in K^+ were greatest in the thalamus (+67 mM), followed by the hippocampus and hypothalamus (44 and 42 mM), and lowest in the cortex (29 mM).

Relationships between temperature, permeability of the BBB and brain water content

As shown in Fig. 4, METH-induced increases in brain water were tightly related to EB leakage (top) and brain temperatures (bottom). Correlation was significant, strong and linear in each studied brain structure. Therefore, the increase in tissue water strongly depends on brain hyperthermia and associated BBB leakage.

Structural changes

Neuronal Changes—As shown in Table 2, METH treatment resulted in a profound increase in the amount of abnormal neural cells in each brain structure. The increase was significant in each region, but the highest numbers were seen in the hippocampus followed by the thalamus, hypothalamus and cortex. The incidence of neuronal damage was almost 1.5 times greater in animals that received METH at 29°C. In this case, the greatest changes were seen in the cortex, followed by hippocampus, thalamus and hypothalamus.

A representative example of Nissl-stained cortical tissue is depicted in Fig. 5. While only healthy neurons with a distinct nucleus and clear cytoplasm were seen in control brains (a), several pyknotic neurons, perineuronal edema, sponginess and expansion of the cortex were seen in METH-treated rats (c and e, arrows). Similar changes were evident in the thalamus and hypothalamus (Fig. 6). Control rats did not show evident neural cell changes (b and c, arrow heads), but the number of dark and distorted neurons with a clear lack of nucleus and condensed cytoplasm was clearly larger in METH-treated rats, especially those in the 29°C group (e, f, h, i). Incidences of perivascular edema (arrowheads) and degeneration of neuropil (*) were also prominent in this group (h, i) compared to METH-23°C group (e, f).

Damage to choroid epithelial cells—METH also induced marked abnormalities in the choroid plexus, determining subsequent breakdown of the blood-cerebrospinal fluid (CSF) barrier. This damage is evident from Fig. 5 (right panels), which shows a Nissl-stained choroid plexus in control (b) and METH-treated rats (d and f). While choroid epithelium in control brains consists of compact and dense epithelial cells with a distinct nucleus (b; arrow-heads), marked degeneration of epithelial cells with occasional staining of cell nuclei were found in METH-23°C rats (d). These changes were most prominent in METH-29°C group, which showed massive degeneration of epithelia with no distinction between individual cell nuclei and epithelial cells (f).

Glial changes—Alterations of glial cells were evaluated using GFAP immunohistochemistry (Table 2). Similar to our previous work (Sharma et al., 1992), few GFAP-positive astrocytes scattered in the normal brains; the hippocampus showed more stained cells than the thalamus, cortex and hypothalamus. In the METH-23°C group, the number of GFAP-positive cells was significantly larger, with the greatest increase in the thalamus followed by the hippocampus, cortex and hypothalamus. In the METH-29°C group, the number of GFAP-positive astrocytes was almost doubled in the cortex and hippocampus and 1.5 times higher in the hypothalamus and thalamus compared to the METH-23°C group. A representative example of GFAP-positive cells during METH treatment is shown in Fig. 2

(c, f, i). While a few GFAP-positive cells (arrowhead) were seen in the control thalamus (c), their numbers were larger in the METH-23°C (f) and especially METH-29°C group (i). In the backgrounds, damaged nerve cells and perineuronal edema were often seen around areas of GFAP expression.

Myelin Changes—In normal animals, myelinated fibers and bundles are stained very dense red with MBP immunostaining (see Fig. 2b) or very dense blue green with Luxol Fast Blue staining (Fig. 6a), showing intact myelin sheaths and myelinated axons. In contrast, degradation of MBP (Fig. 2e) and Luxol Fast Blue staining (Fig. 6d, g) seen in METH-treated animals reflects markedly damaged myelinated fibers and axons. This decrease in myelin was further aggravated in the METH-29°C group (see Fig. 2h and Fig. 6g). Degeneration of myelin was commonly seen in the areas showing edematous expansion of the neuropil (Fig. 2h).

Relationships between brain damage and other parameters—Changes in brain morphology were related to changes in all other analyzed parameters (Table 1 and 2 and Fig. 7). As can be seen in Fig. 7A, cortical cell abnormalities during METH intoxication were tightly related to both *body* and *brain hyperthermia*. A strong relationship seen for the cortex was equally evident for each other studied structure. While the counts of damaged cells were progressively larger with temperature increase, the intensity of damage in each structure was independent of absolute temperatures. While in this study, brain temperature was recorded only from the NAcc, it should follow a dorso-ventral temperature gradient and be lowest in the cortex, higher in the hippocampus and thalamus, and highest in the hypothalamus (see Kiyatkin, 2005). However, METH-induced cell abnormalities were minimal in the “warm” hypothalamus, but maximal in the “cool” cortex.

METH-induced changes in brain morphology occurred very rapidly (range 66–94 and 26–79 min in METH-23 and METH-29°C, respectively) and were independent of *time of METH exposure*. Despite much larger damage in METH-29°C than in METH-23°C, the mean time of exposure was shorter (81.88±3.96 vs. 58.13±5.82 min). No correlation with exposure time was found in each of the two groups analyzed separately (r=0.16 for 23°C and r=0.06 for 29°C).

As can be seen in Fig. 7B, cortical neuronal damage tightly correlates with *increased permeability of BBB to EB*, which was maximal in this brain structure. This relationship is well approximated by a liner regression line (r=0.923). Similarly strong linear correlations were found in three other structures (r=0.913, 0.951 and 0.928 for the hippocampus, thalamus and hypothalamus, respectively). Brain damage was also strongly correlated with the intensity of *albumin immunostaining* both in the cortex (Fig. 7C) and all other structures (r=0.902, 0.892 and 0.899 for the hippocampus, thalamus and hypothalamus, respectively).

The number of damaged cells during METH intoxication linearly correlates with *water accumulation* in both the cortex (Fig. 7D) and other brain areas. This relation appears to be a reflection of generalized edema, which is stronger with METH used at 29°C, resulting in more profound cellular damage.

Finally, the number of distorted cortical neurons linearly correlates with the number of GFAP-positive glial cells (Fig. 8C). This correlation was also evident in all other structures (r=0.900, 0.902 and 0.903 for the hippocampus, thalamus and hypothalamus, respectively), pointing at its generality for the brain as a whole.

Ultrastructural changes following METH administration

Cellular changes seen at light microscopy were further confirmed using transmission electron microscopy (TEM, Figs. 8–10).

Neuronal changes—At the ultrastructural level, several neuronal profiles located in the cortex were examined with special emphasis on the neuronal nucleolus and karyoplasm (see Fig. 8). In control rats (a), neurons had a perfectly smooth, rounded nuclear membrane containing centralized nucleolus (arrow); the surrounding cytoplasm normally did not contain any vacuole, and the adjacent neuropil was quite compact. In contrast, degeneration of the nucleolus, which became slightly eccentric (c), numerous foldings of the nuclear membrane, vacuolation in the neuronal cytoplasm (*), and degenerative changes in perinuclear membranes were seen in cortical tissue in the METH-23°C group (c). These changes were more profound in animals that receive METH at 29°C (e). In this case, the nucleolus reached to the one end of the karyoplasms, the nuclear envelope showed many irregular foldings (e), and the cytoplasm was vacuolated (*), often with degeneration of the Nissl substance.

Axonal changes—Damage of myelin and axons seen in METH-treated animals using light microscopy with MBP and Luxol Fast Blue staining was further confirmed at the ultratstructural level. The most marked changes in myelin vesiculation were seen in rats treated with METH at 29°C compared to those that received this drug at 23°C (Fig. 8d, f). Unlike control animals (Fig. 8b) which exhibited a compact neuropil and normal mylelin sheath around the axons (arrowheads), METH-treated rats showed clear signs of damage to myelinated axons (d: arrows show myelin vesiculation and * shows axonal damage), which was more pronounced in animals that received METH at 29°C (f). Degeneration of myelinated axons, vesiculation of myelin (f, arrows), and edematous swelling of axonal membranes (f, *) were frequent in this group.

Changes in the neuropil—Ultrastructural changes in the neuropil were examined at high magnification in the cortex and hippocampus of METH-treated animals (Fig. 9). In contrast to normal compact neuropil in control animals, membrane damage, vacuolation (a, *), degeneration of axons (d, arrow) and possibly dendrites (b, arrow), as well as the signs of edema and sponginess were typically seen in rats treated with METH (a, b, c, d). The intensity of these pathological changes was clearly stronger in the METH-29°C than METH-23°C groups (compare a–b with c–d).

Endothelial cell and glial changes—Several endothelial cell profiles and the surrounding neuropil in the cortex and hippocampus were examined at the ultrastructural level (Fig. 10). As can be seen, the control brains had a compact neuropil and perivascular structures, the endothelial cell surface of the lumen is very smooth, and tight junctions (arrow) are clearly distinct (a, b). In animals exposed to METH, the endothelial cell surface in the lumen was markedly altered (c, d) with many endothelial cell bleb formations (d, arrowhead). The perivascular edema (*) and membrane vacuolation in the neuropil was also apparent (c, d). These perivascular changes and endothelial cell membrane reactions were much more aggravated in animals that received METH at 29°C (e, f, arrowheads). In these rats, perivascular glial cells were swallen (*) and pericapilary neuropil was degenerated (e, f). The endothelial cell membrane showed prominent bleb formation in this group, and the endothelial cell cytoplasm was more electron dense (e, f) than the normal endothelium (a, b). However, the tight junctions appear to be intact in all METH-treated group.

Discussion

While slowly developing, selective, and irreversible damage of specific central neurons is a traditional focus of METH neurotoxicity research, this work demonstrates that robust morphological abnormalities of neural and non-neural brain cells (i.e., glia, vascular endothelium, epithelium) could occur in various brain structures very rapidly (within 30–80 min) during acute METH intoxication, not reported earlier. These abnormalities manifest as the distortion of neurons, overexpression of glial cells, vesiculation of myelin and alterations

in vascular endothelium and epithelium of the choroid plexus. While having some structural specificity, these acute morphological abnormalities appear to be widespread, tightly correlating with drug-induced brain and body hyperthermia and alterations in several basic homeostatic brain parameters, including water and ion contents. This study is the first to focus on the relationships between these structural and functional alterations to clarify the pathophysiological mechanisms underlying brain abnormalities during acute METH intoxication. While this issue is crucial for understanding this life-threatening human condition, brain abnormalities resulting from acute METH exposure may contribute to a slowly developing, irreversible neurodegeneration that could occur following chronic METH abuse.

Mechanisms underlying METH-induced morphological brain abnormalities

Hyperthermia is the most important symptom of acute METH intoxication and a factor implicated in neurotoxicity (Bowyer et al., 1994; Miller and O'Callaghan, 1994, 2003; Alberts and Sonsalla, 1995; Yuan et al., 2006). The present study revealed that acute morphological alterations of brain cells during METH intoxication are tightly related to drug-induced increases in brain and muscle temperatures. The tight link between hyperthermia and structural brain damage was evident in different brain structures and for both neuronal (Nissl staining), glial (GFAP immunoreactivity), endothelial (TEM) and epithelial (Nissl staining and TEM) cells. To establish the relationships between drug-induced functional and structural abnormalities and brain temperature, all rats received METH at the same dose but at different ambient temperatures, which affected heat dissipation from the brain and modulated drug-induced brain hyperthermia within a wide range. Therefore, although all animals had a similar metabolic impact of the drug, they showed different brain hyperthermia (37.5–42.0°C) because of both complications in dissipation of metabolic heat (29°C) and individual variability in both subgroups. Although we always tried to take the brains when temperatures peaked, in some rats in the 29°C group brains were taken at extreme hyperthermia (>41.5°C) or at a possible pre-terminal state, when the rats decreased locomotor activity, showed intense stereotypy and, sometimes, weak convulsions but were alive. We were confident that some of these animals would not have survived if the experiment continued. Such an approach allowed us to examine different brain parameters within a wide range of fluctuations from normal (in control rats) to clearly pathological. Thus, in addition to group analysis (control, METH-23°C and METH-29°C), we also examined the quantitative relationships between various brain parameters within the whole range of physiological and pathological variations.

It is well known that high temperature has destructive effects on various cells (Iwagami, 1996; Willis et al., 2000; Du et al., 2007), especially strong on metabolically active brain cells (Chen et al., 2003; Oifa and Kleshchenov, 1985; Lin et al., 1991; Lin, 1997; Lee et al., 2000), including glial, endothelial and epithelial cells (Bechtold and Brown, 2003; Sharma and Hoopes, 2003). Therefore, robust differences in the amounts of structurally damaged neurons and abnormal GFAP-positive cells as well as a linear correlation between these parameters and NAcc temperature could suggest brain hyperthermia as an important contributor to METH-induced morphological abnormalities. However, this does not mean that high temperature *per se* is the cause of these changes. Brain hyperthermia is not only a physical factor that could harm cells, it is also an integral physiological index of METH-induced metabolic activation (see Kiyatkin, 2005 for review), which also manifests as an enhanced release of multiple neuroactive substances, lipid peroxidation and the generation of free radicals—numerous changes combined as oxidative stress (Seiden and Sabol, 1996; Cadet et al., 2007) as well as behavioral and autonomic activation. Although all these factors may contribute to structural brain abnormalities and their harmful effects are known to be enhanced by high temperature, it is quite difficult to separate them from each other because they are interdependent, representing different manifestations of METH-induced metabolic activation.

Extending our previous observations (Kiyatkin et al., 2007), this study demonstrates that METH intoxication results in a robust increase in BBB permeability, intra-brain water accumulation (edema) and serious shifts in brain ionic homeostasis. These changes, moreover, were tightly related to both the degree of hyperthermia and the intensity of structural brain damage in each of four studied structures. While in normal conditions, albumin is confined to the luminal side of endothelial cells (Sharma, 2004) and the exogenous protein tracer EB which binds to plasma albumin and fails to enter the brain from the peripheral circulation (Blezer, 2005; Ehrlich, 1904), both of these parameters strongly increased in each brain structure during METH-intoxication and the increase was much more pronounced (sometimes greater than 2x), when METH was used at 29°C and elevations in internal temperatures were larger. Therefore, METH, by enhancing BBB permeability, allows endogenous albumin, several ions and other neuroactive and potentially neurotoxic substances to enter the brain inevitably resulting in water accumulation in brain tissue (vasogenic edema) and serious shifts in ionic brain homeostasis (see Rapoport, 1976; Sharma, 2006 for review). Therefore, these factors could be also viewed as important contributors to brain pathology and the primary mechanism underlying decompensation of vital functions and lethality. While different chemical factors activated by METH could be involved in increased BBB permeability and edema formation, brain hyperthermia appears to play a crucial role because both the count of albumin-positive cells and tissue water strongly correlated with brain temperature in each brain structure.

Common features and structural selectivity of METH-induced cellular alterations

To define the common features and structural specificity of METH-induced morphological and functional perturbations, our examinations were conducted in the cortex, hippocampus, thalamus, and hypothalamus examined at the level of the diencephalon. These structures had some differences in tested parameters in normal conditions and, despite significant between-group differences, also showed some degree of specificity following METH impact (see Table 1 and 2). While individual structures differed in tissue water content in control brains, its increase was relatively similar in each structure at 23°C (~1.3%; see Table 1) and dramatically amplified at 29°C (~2.6–3.1%), suggesting severe edema. Robust water accumulation in brain tissue was associated with a clearly pathological brain hyperthermia (>41°C), strong increases in Na^+, K^+, Cl^- in all brain structures, and maximal increases in albumin- (x22–75) and GFAP-positive (x8–13) cells. These animals also showed especially strong cellular abnormalities, which were evident in each structure and with each morphological and histochemical test. Degeneration of cellular elements in the nucleus, condensed cytoplasm, and irregular folding of the nuclear membrane found with electron microscopy denotes clear cell damage, which would possibly lead to future cellular disintegration. While our experiment was stopped at a certain time point and we cannot project the fate of acutely damaged cells, it could be reasonably assumed that these robust pathological brain perturbations could result in profound functional disturbances and lethality. Although edema and ionic misbalance appears to be widespread within the brain, individual structures differed in the extent of morphological abnormalities. The quantities of damaged neuronal and glial cells were equally greater in the cortex and hippocampus, but smaller in the thalamus and hypothalamus. While the reasons behind this structural specificity to damage remain unknown, the cortex and hippocampus also showed much stronger increases in EB penetration and albumin immunostaining than the thalamus and hypothalamus, suggesting a tight link between BBB leakage and structural damage. Although brain damage was evident in each cellular subtype (neurons, glial cells, vascular endothelium, axons), especially profound abnormalities were found in epithelial cells of the choroid plexus —a critical substrate of the blood-cerebrospinal fluid (CSF) barrier (Keep et al., 2005). Because of the role of this organ in production of the CSF, damage of epithelial cells and destruction of gap junctions could strengthen edema and ionic disbalance, thus amplifying cellular damage in other brain structures. While it is unclear why this structure is so sensitive to damage during METH intoxication, it has an exceptionally high blood flow (Faraci et al., 1988) and

mitochondrial density (Keep and Jones, 1990) compared to other structures, supporting a presumed link between local metabolic activity and cellular damage following thermal impact (see Kiyatkin, 2005 for review).

Reversibility of structural alterations and their mechanisms

Although our data for the first time indicate that METH intoxication results in rapidly developing morphological abnormalities in neural and non-neural brain cells, it remains unclear whether these abnormalities are reversible or irreversible. Dramatic changes in cellular elements (e.g., degeneration of some neuronal nucleus, endothelial cell membrane bleb-formation, vesiculation of myelin and vacuolation in the neuropil with clear signs of synaptic damage and swelling), especially evident in the METH-29°C, appear to be inconsistent with normal cell functions, pointing at irreversible damage and possible future cell destruction. However, significant time is always necessary for a normal cell to become damaged, for the damage to become irreversible, and for an irreversibly damaged cell to die and to be recognized as dead. Moreover, dead cells are effectively eliminated from brain tissue by phagocytosis and their detection in brain tissue has a certain time window and requires the use of specific techniques. Finally, some brain cells could be repaired or replaced by regenerated ones.

One the other hand, some of these morphological changes could be transient and reversible, disappearing after basic homeostatic parameters are restored to baseline. In contrast to the unusually large numbers of GFAP-positive glial cells found in this study during acute METH intoxication (x3–7 and x7–12 vs. control in 23 and 29°C groups, respectively), much weaker increases in GFAP-positive cells were found in rats in days after acute METH impact (Miller and O'Callaghan, 1994; O'Callaghan and Miller, 1994). These changes, moreover, appeared at 12–24 hrs, peaked at the second day, and remained elevated for 7 days after a single high-dose METH exposure. In contrast to widespread effect in our study, these changes were evident only in the striatum and to a lesser degree in the cortex, correlating with decreased dopamine levels in these structures.

In contrast to the relatively slow and weak changes in GFAP immunoreactivity found in days after acute METH treatment, rapid and strong increases in GFAP immunostaining have been previously reported during environmental warming (~2–3 hours; Sharma et al., 1992; Cervos-Navarro et al., 1998) and following acute traumatic injury to the brain and spinal cord (30–40 min; Gordth et al., 2006; Sharma et al., 1998), suggesting that the mechanisms underlying rapid and slow glial reaction could be quite different. GFAP expression is usually thought as a late outcome of traumatic, ischemic or hypoxic insults or a correlate of various neurodegenerative diseases (Finch, 2003; Hausmann, 2003; Gordh et al., 2006), representing astrogliosis (Norton et al., 1992; O' Callaghan, 1993). In contrast, rapid GFAP expression seen in association with strong edema (environmental warming, acute trauma, METH intoxication) could reflect the interaction of antibodies with GFAP somehow released or made available during membrane damage. Thus, binding sites to GFAP could be increased *due to* high hyperthermia, acute breakdown of the BBB and associated edema, rather than proliferation of astrocytes or elevated levels of GFAP proteins that require more time. Since damage of astrocytes and swelling of the astrocytic end feet result in increased binding of GFAP antibodies (Bekay et al., 1977; Bondarenko and Chesler, 2001; Gordh et al., 2006), this reaction could reflect acute and possibly reversible damage of glial cells. Although the issues of the damage extent and its reversibility remains unanswered and required additional studies, it is likely that rapid cell abnormalities may initiate cascades that could precipitate cellular and molecular dysfunctions, leading to early neurodegeneration—the most dangerous outcome of chronic abuse with amphetamine-like drugs.

Acknowledgements

This study was supported by the Intramural Research Program of NIDA-NIH, the Leaderal Foundation, and 2006 NIDA Distinguished International Scientist Collaboration Award (NIH) awarded to Hari S. Sharma. The authors greatly appreciate technical assistance of Mari-Anne Carlsson and Inga Hörte (Uppsala University) as well as P. Leon Brown (NIDA-IRP).

Abbreviations

NAcc
nucleus accumbens

BBB
blood-brain barrier

EB
Evans blue

METH
methamphetamine

GFAP
glial fibrillary acidic protein

CSF
cerebro-spinal fluid

MBP
myelin basic protein

TEM
transmission electronic microscopy

References

Alberts DS, Sonsalla PK. Methamphetamine-induced hyperthermia and dopaminergic neurotoxicity in mice: Pharmacological profile of protective and nonprotective agents. J Pharmacol Exp Ther 1995;275:1104–1114. [PubMed: 8531070]

Ali SF, Newport GD, Slikker W. Methamphetamine-induced dopaminergic toxicity in mice: Role of environmental temperature and pharmacological agents. Ann NY Acad Sci 1996;801:187–198. [PubMed: 8959033]

Bechtold DA, Brown IR. Induction of Hsp27 and Hsp32 stress proteins and vimentin in glial cells of the rat hippocampus following hyperthermia. Neurochem Res 2003;28:1163–1173. [PubMed: 12834255]

Bekay L, Lee JC, Lee GC, Peng GR. Experimental cerebral concussion: An electron microscopic study. J Neurosurg 1977;47:525–531. [PubMed: 903805]

Blezer, E. Techniques for measuring the blood-brain barrier integrity. In: de Vries, E.; Prat, A., editors. the Blood-Brain Barrier and Its Microenvironment. New York: Taylor & Francis; 2005. p. 441-456.

Bondarenko A, Chesler M. Rapid astrocyte death induced by transient hypoxia, acidosis, and extracellular ion shifts. Glia 2001;34:134–142. [PubMed: 11307162]

Bowyer JF, Davies DL, Schmued L, Broening HW, Newport GD, Slikker W, Holson RR. Further studies of the role of hyperthermia in methamphetamine neurotoxicity. J Pharmacol Exp Ther 1994;268:1571–1580. [PubMed: 8138969]

Bowyer JF, Ali S. High doses of methamphetamine that cause disruption of the blood-brain barrier in limbic areas produce extensive neuronal degeneration in mouse hippocampus. Synapse 2006;60:521–532. [PubMed: 16952162]

Brown PL, Kiyatkin EA. Fatal intra-brain heat accumulation induced by meth-amphetamine at normothermic conditions in rats. Int J Neurodegener Neuroregener 2005;1:86–90.

Brown PL, Wise RA, Kiyatkin EA. Brain hyperthermia is induced by methamphetamine and exacerbated by social interaction. J Neurosci 2003;23:3924–3929. [PubMed: 12736362]

Cadet JL, Jayanthi S, Deng X. Methamphetamine-induced neuronal apoptosis involves the activation of multiple death pathways. Neurotox Res 2005;8:199–206. [PubMed: 16371314]

Cadet JL, Krasnova IN, Jayanthi S, Lyles J. Neurotoxicity of substituted amphetamines: molecular and cellular mechanisms. Neurotox Res 2007;11:183–202. [PubMed: 17449459]

Cerves-Navarro J, Sharma HS, Westman J, Bongcum-Rudloff E. Glial cell reactions in the central nervous system following heat stress. Progr Brain Res 1998;115:241–274.

Chen YZ, Xu RX, Huang QJ, Xu ZJ, Jiang XD, Cai YO. Effect of hyperthermia on tight junctions between endothelial cells of the blood-brain barrier model in vitro. Di Yi Jun Da Xue Xue Bao 2003;23:21–24.

Derlet RW, Albertson TE, Rice P. Antagonism of cocaine, amphetamine, and methamphetamine toxicity. Pharmacol Biochem Behav 1990;36:745–749. [PubMed: 2217500]

Du J, Di HS, Wang GL. Establishment of a bovine mammary cell line and its ultrastructural changes when exposed to heat stress. Sheng Wu Gong Cheng Xue Bao 2007;23:471–476. [PubMed: 17577996]

Ehrlich, P. Uber die Beziehung chemischer onstitution, Verteilung, und pharmacologischer Wirkung. Gesammelte Arbeiten zur Immunitatsforschung; Berlin. 1904.

Estler CJ. Dependence on age of metamphetamine-produced changes in thermoregulation and metabolism. Experientia 1975;31:1436–1437. [PubMed: 1213067]

Faraci FM, Mayham WG, Williams JK, Heistad DD. Effects of vasoactive stimuli on blood flow to choroid plexus. Am J Physiol 1988;254:H286–H291. [PubMed: 3344819]

Finch CE. Neurons, glia, and plasticity in normal brain aging. Neurobiol Aging 2003;24(Suppl 1):S123–127. [PubMed: 12829120]

Gordh T, Chu H, Sharma HS. Spinal nerve lesion alters blood-spinal cord barrier function and activates astrocytes in the rat. Pain 2006;124:211–221. [PubMed: 16806707]

Hausmann ON. Post-traumatic inflammation following spinal cord injury. Spinal Cord 2003;41:369–378. [PubMed: 12815368]

Iwagami Y. Changes in the ultrastructure of human cell related to certain biological responses under hyperthermic culture conditions. Human Cell 1996;9:353–366. [PubMed: 9183669]

Joo F, Szucs A, Csanda E. Netiamine treatment of brain oedema in animals exposed to 90-yttrium radiation. J Pharm Pharmacol 1976;328:162–163. [PubMed: 6680]

Kalant H, Kalant OJ. Death in amphetamine users: causes and rates. Can Med Assoc J 1975;112:299–304. [PubMed: 1089034]

Keep RF, Jones HC. A morphometric study on the development of the lateral choroids plexus, choroids plexus capillaries and ventricular ependyma in the rat. Dev Brain Res 1990;56:47–53. [PubMed: 2279331]

Keep, RF.; Ennis, SR.; Xiang, J. The blood-CSF barrier and cerebral ischemia. In: Zheng, W.; Chodobski, A., editors. The blood-cerebrospinal fluid barrier. Boca Raton: CRC Press; 2005. p. 345-360.

Kiyatkin EA. Brain hyperthermia as physiological and pathological phenomena. Brain Res Rev 2005;50:27–56. [PubMed: 15890410]

Kiyatkin EA, Brown PL, Sharma HS. Brain edema and breakdown of the blood-brain barrier during methamphetamine intoxication: critical role of brain temperature. Eur J Neurosci 2007;26:1342–1353.

Lee SY, Lee SH, Akuta K, Uda M, Song CW. Acute histological effects of interstitial hyperthermia on normal rat brain. Int J Hyperthermia 2000;16:73–83. [PubMed: 10669318]

Lin PS, Quamo S, Ho KC, Gladding J. Hyperthermia enhances the cytotoxic effects of reactive oxygen species to Chinese hamster cells and bovine endothelial cells *in vitro*. Radiat Res 1991;126:43–51. [PubMed: 1850533]

Lin MT. Heatstroke-induced cerebral ischemia and neuronal damage. Involvement of cytokines and monoamines. Ann NY Acad Sci 1997;813:572–580. [PubMed: 9100936]

Makisumi T, Yoshida K, Watanabe T, Tan N, Murakami N, Morimoto A. Sympatho-adrenal involvement in methamphetamine-induced hyperthermia through skeletal muscle hypermethanolism. Eur J Pharmacol 1998;363:107–112. [PubMed: 9881575]

Miller DB, O'Callaghan JP. Environment-, drug- and stress-induced alterations in body temperature affect the neurotoxicity of substituted amphetamines in the C57BL/6J mouse. J Pharmacol Exp Ther 1994;270:752–760. [PubMed: 8071868]

Miller DB, O'Callaghan JP. Elevated environmental temperature and methamphetamine neurotoxicity. Environ Res 2003;92:48–53. [PubMed: 12706754]

Norton WT, Aquino DA, Hozumi I, Chiu FC, Brosnan CF. Quantitative aspects of reactive gliolis: A review. Neurochem Res 1992;17:877–885. [PubMed: 1407275]

O'Callaghan JP. Quantitative features of reactive gliolis following toxicant-induced damage of the CNS. Ann NY Acad Sci 1993;679:195–210. [PubMed: 8512183]

O'Callaghan JP, Miller DB. Neurotoxicity profiles of substituted amphetamines in the C57BL/6J mouse. J Pharmacol Exp Ther 1994;270:741–751. [PubMed: 8071867]

Oifa AI, Kleshchnov VN. Ultrastructural analysis of the phenomenon of acute neuronal swelling. Zh Nevropatol Psikhiatr Im SS Korsakova 1985;85:1016–1020.

Paxinos, G.; Watson, C. The Rat Brain in Stereotaxic Coordinates. Vol. 4. San Diego: Academic Press; 1998.

Rapoport, SI. Blood-brain barrier in physiology and medicine. Raven Press; New York: 1976.

Ricaurte GA, Schuster CR, Seiden LS. Long-term effects of repeated methamphetamine administration on dopamine and serotonin neurons in the rat brain: a regional study. Brain Res 1980;193:153–163. [PubMed: 7378814]

Sandoval V, Hanson GR, Fleckenstein AE. Methamphetamine decreases mouse striatal dopamine transport activity: roles of hyperthermia and dopamine. Eur J Pharmacol 2000;409:265–271. [PubMed: 11108820]

Seiden LS, Sabol KE. Methamphetamine and methylenedioxymethamphetamine neurotoxicity: possible mechanisms of cell destruction. NIDA Res Monogr 1996;163:251–276. [PubMed: 8809863]

Sharma, HS. Blood-brain and spinal cord barriers in stress. In: Sharma, HS.; Westman, J., editors. Blood-Spinal Cord and Brain Barriers in Health and Disease. Academic Press; San Diego: 2004. p. 231-298.

Sharma HS. Hyperthermia-induced brain oedema: Current status and future perspectives. Indian J Med Res 2006;123:629–652. [PubMed: 16873906]

Sharma HS, Ali SF. Alterations in blood-brain barrier function by morphine and amphetamine. Ann NY Acad Sci 2006;1074:198–224. [PubMed: 17105918]

Sharma HS, Cervos-Navarro J. Brain edema and cellular changes induced by acute heat stress in young rats. Acta Neurochir Suppl (Wein) 1990;51:383–386.

Sharma HS, Hoopes PJ. Hyperthermia-induced pathophysiology of the central nervous system. Int J Hyperthermia 2003;19:325–54. [PubMed: 12745974]

Sharma HS, Kretzschmar R, Cervos-Navarro J, Ermisch A, Ruhle HJ, Dey PK. Age-related pathophysiology of the blood-brain barrier in heat stress. Prog Brain Res 1992;91:189–196. [PubMed: 1410403]

Sharma HS, Olsson Y, Cervós-Navarro J. Early perifocal cell changes and edema in traumatic injury of the spinal cord are reduced by indomethacin, an inhibitor of prostaglandin synthesis. Acta Neuropathologica (Berlin) 1993;85:145–153. [PubMed: 8442406]

Sharma HS, Olsson Y, Pearsson S, Nyberg F. Trauma induced opening of the blood-spinal cord barrier is reduced by indomethacin, an inhibitor of prostaglandin synthesis. Experimental observations in the rat using 131I-sodium, Evans blue and lanthanum as tracers Restor. Neurol Neurosci 1995;7:207–215.

Sharma HS, Sjöquist PO. A new antioxidant compound H-290/51 modulates glutamate and GABA immunoreactivity in the rat spinal cord following trauma. Amino Acids 2002;23:261–72. [PubMed: 12373546]

Sharma HS, Westman J, Nyberg F. Pathophysiology of brain edema and cell changes following hyperthermic brain injury. Progr Brain Res 1998;115:351–412.

Sharma HS, Zimmer C, Westman J, Cervos-Navarro J. Acute systemic heat stress increases glial fibrillary acidic protein immunoreactivity in brain. An experimental study in the conscious normotensive young rats. Neuroscience 1992;48:889–901. [PubMed: 1630627]

Thomas DM, Dowgiert J, Geddes TJ, Francescutti-Verbeem D, Liu X, Kuhn DM. Microglial activation as a pharmacologically specific marker for the neurotoxic amphetamines. Neurosci Lett 2004;367:349–354. [PubMed: 15337264]

Willis WT, Jackman MR, Bizeau ME, Pagliassotti MJ, Hazel JR. Hyperthermia impairs liver mitochondrial functions. Am J Physiol 2000;278:R1240–1246.

Yamamoto BK, Bankson MG. Amphetamine neurotoxicity: cause and consequence of oxidative stress. Crit Rev Neurobiol 2005;17:87–117. [PubMed: 16808729]

Yuan J, Hatzidimitriou G, Suthar P, Mueller M, McCann U, Richarte G. Relationships between temperature, dopaminergic neurotoxicity, and plasma drug concentrations in methamphetamine-treated squirrel monkeys. J Pharmacol Exp Ther 2006;316:1210–1218. [PubMed: 16293712]

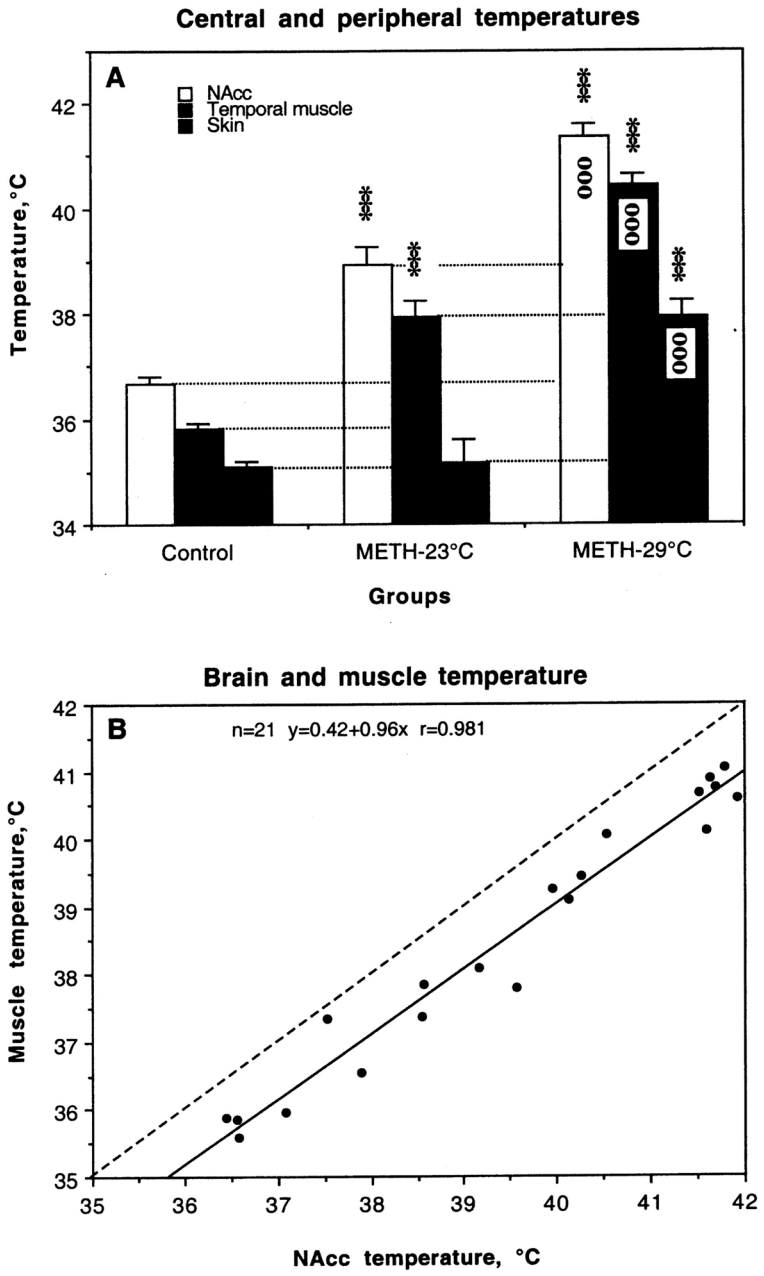

Fig. 1.

A. Changes in NAcc, muscle and skin temperatures induced by methamphetamine (METH, 9 mg/kg, sc) administered at standard (23°C) and warm (29°C) ambient temperatures. Asterisks show values significantly different from control (120 min after a sc saline injection at 23°C) and small circles show differences between two METH groups (***, ooo, $p<0.001$; Student's t-test). B. Relationships between temperatures in the NAcc and temporal muscle assessed in all animals used in this study.

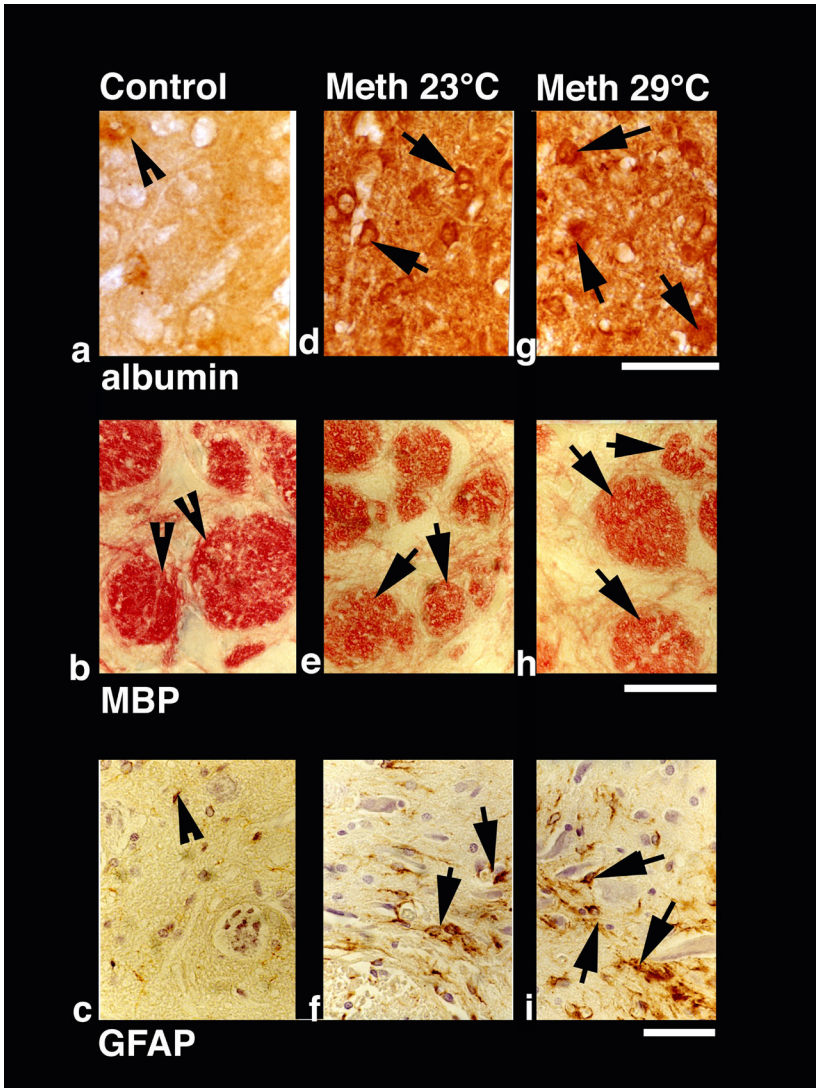

Fig. 2.

Immunohistochemical changes in albumin (a, d, g), myelin basic protein (MBP; b, e, g) and glial fibrillary acidic protein (GFAP; c, f, i) in control (left vertical panel) and METH-treated rats (23°: middle vertical panel and 29°C: right vertical panel). Compared to weak albumin immunoreactivity in control (a, arrowhead), METH-treated rats had stronger immonoreactivity (arrows in d and g). Expansion of neuropil and sponginess is also evident in the surrounding background. Bar (a,d,g) = 40 μm. In contrast to intense red myelin bundles and dense red fibers in control (b, arrowheads, b), diminution of red staining in the bundles and fibers (e, arrows) was seen in METH-treated rats (e). This degradation of MBP was most prominent in the rats treated with METH at 29° C (arrows, h). Bar (b, e, h) = 30 μm. GFAP immunostaining was prominent in METH-treated rats at 29° C (i, arrows) compared to 23°C (f, arrows). Control rats (c) occasionally show few GFAP positive astrocytes (arrowhead). Reactive astrocytes were located around the nerve cells and microvessels and were distributed in wide regions in the neuropil. Damaged neurons can also be seen in the background. Bar (c, f, i) = 40 μm.

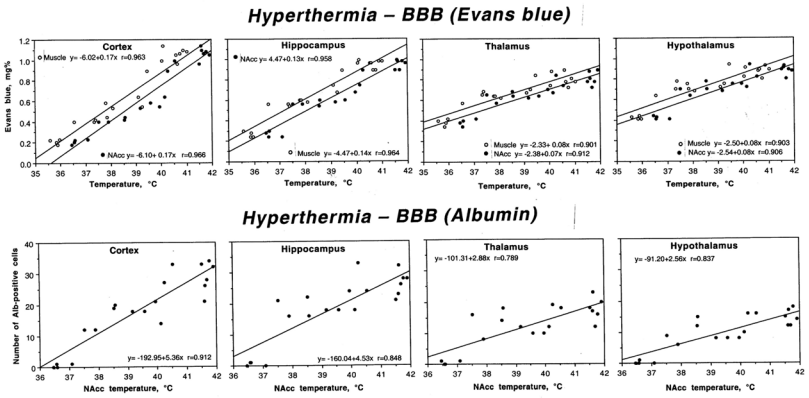

Fig. 3.

Relationships between brain temperature (°C) and two parameters of BBB permeability (local concentrations of Evans blue, mg% and the number of Albumin-positive cells per section) in different brain structures during acute METH intoxication. Upper row also shows muscle temperature. Each graph shows a regression line, regression equation, and coefficient of correlation.

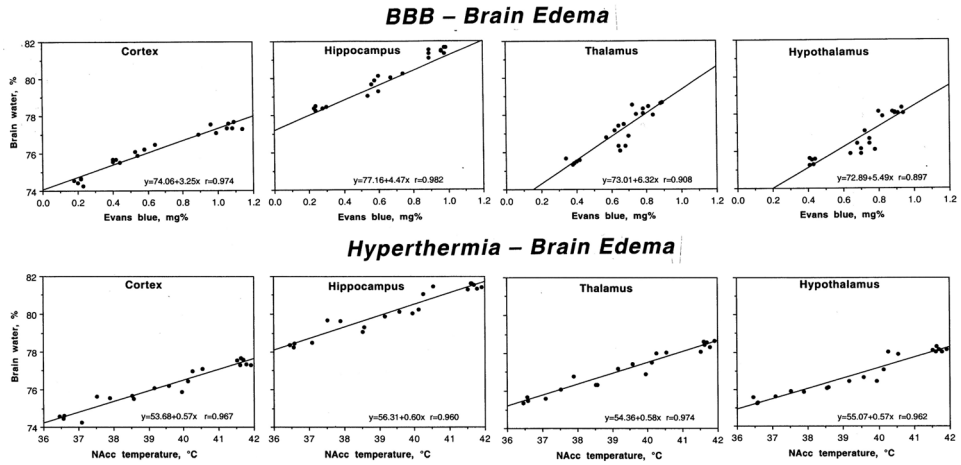

Fig. 4.

Relationships between permeability of the BBB (Evans blue, mg%) and brain edema (water, %) and between brain hyperthermia (NAcc temperature, °C) and edema in different brain structures during acute METH intoxication. Each graph shows a regression line, regression equation, and coefficient of correlation.

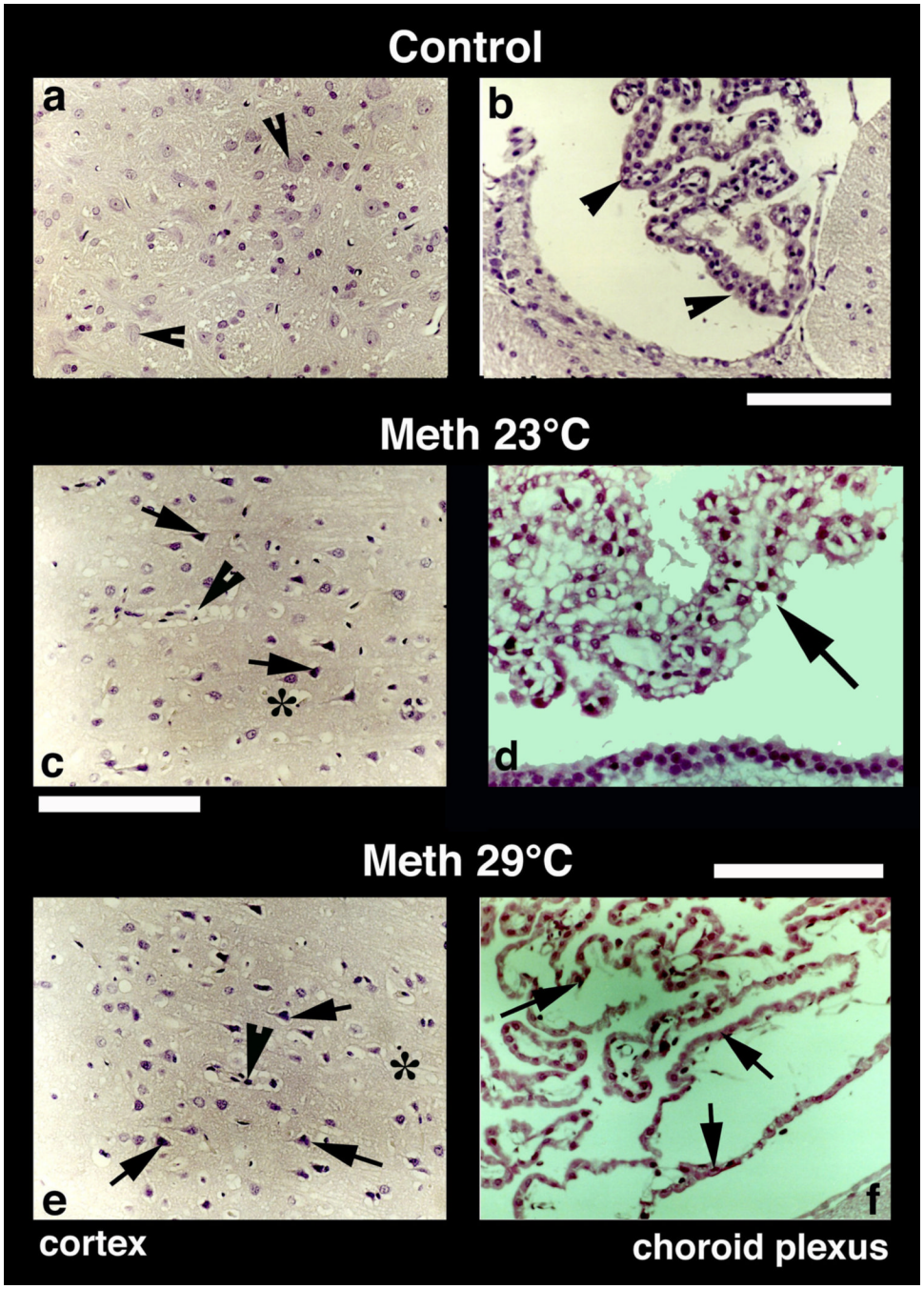

Fig. 5.

Nissl-stained sections from the cerebral cortex (left panel) and choroid plexus (right panel) from control (a, b), METH-23°C (c, d) and METH-29°C (e, f) treated rats. Most of the nerve cells in the control cortex are healthy with a distinct nucleus in the center. Only a few nerve cells show a condensed cytoplasm (arrowheads, a). On the other hand, dark and distorted neurons were frequent in METH-treated rats (c and e; arrows). Sponginess (*) and perivascular edema (arrowheads; c, e) are frequent in METH-treated rats; the changes are more pronounced at 29° C (e) compared to 23° C (c). Bars (a, c, e) = 50 μm. Nissl-stained choroid epithelial cells in control (b) show compact and densely packed epithelial cells with a distinct cell nucleus (arrow, b). METH treatment at 23° C resulted in mild degeneration of choroid epithelium

(arrows, d). The epithelial cell nucleus also appears to be disintegrated (d). These degenerating changes in the choroidal epithelium is most pronounced in the rat that received METH at 29° C (arrows, f). Bars (b = 50 μm; d = 40 μm, f = 60 μm).

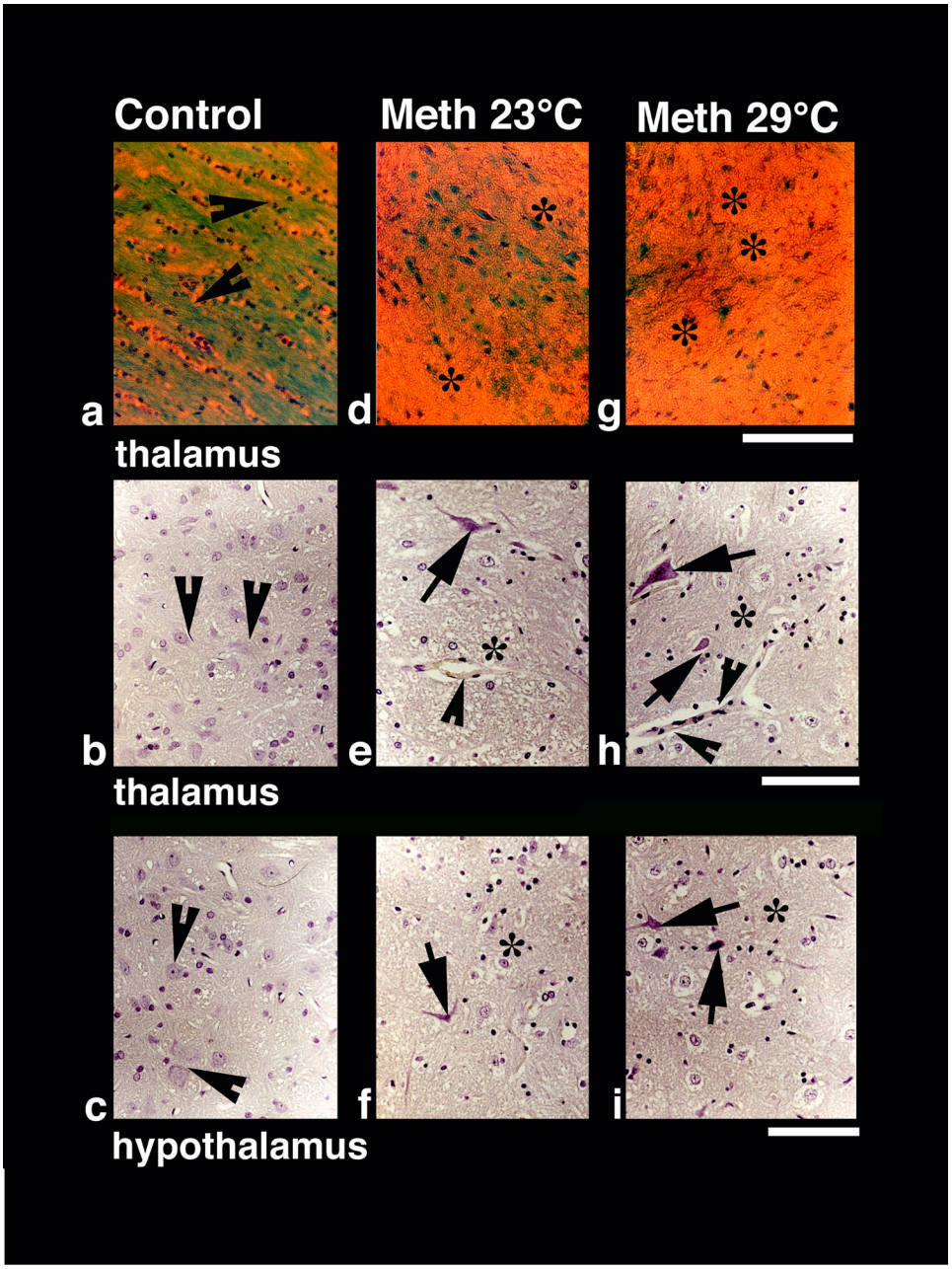

Fig. 6.

Luxol Fast blue (upper panel) and Nissl staining (middle and lower panels) in control (a–c), METH-23°C (d–f) and METH 29°C (g–i) treated rats. Dense myelinated axons and fibers (arrow heads, a) stained by Luxol Fast Blue seen in control (a) diminished in the METH-23° C group (d) and generally lost in METH-29°C group (g). Sponginess and edema (*) is seen in the background of Luxol Fast Blue-stained elements (d, g). Bar = 50 μm. Nissl-stained nerve cells show pronounced degenerative changes in the thalamus (middle panel) and hypothalamus (lower panel) that are stronger in METH-29°C (arrows, h, i) than METH=23°C group (arrows, e, f). Control animals showed healthy neurons with a distinct nucleus in both the thalamus (arrow heads b) and hypothalamus (arrow heads c). Perivascular edema (arrowhead e) and sponginess (*) are most marked in the METH-29°C group (h, i). Bars (b, e, h = 40 μm; c, f, i = 40 μm).

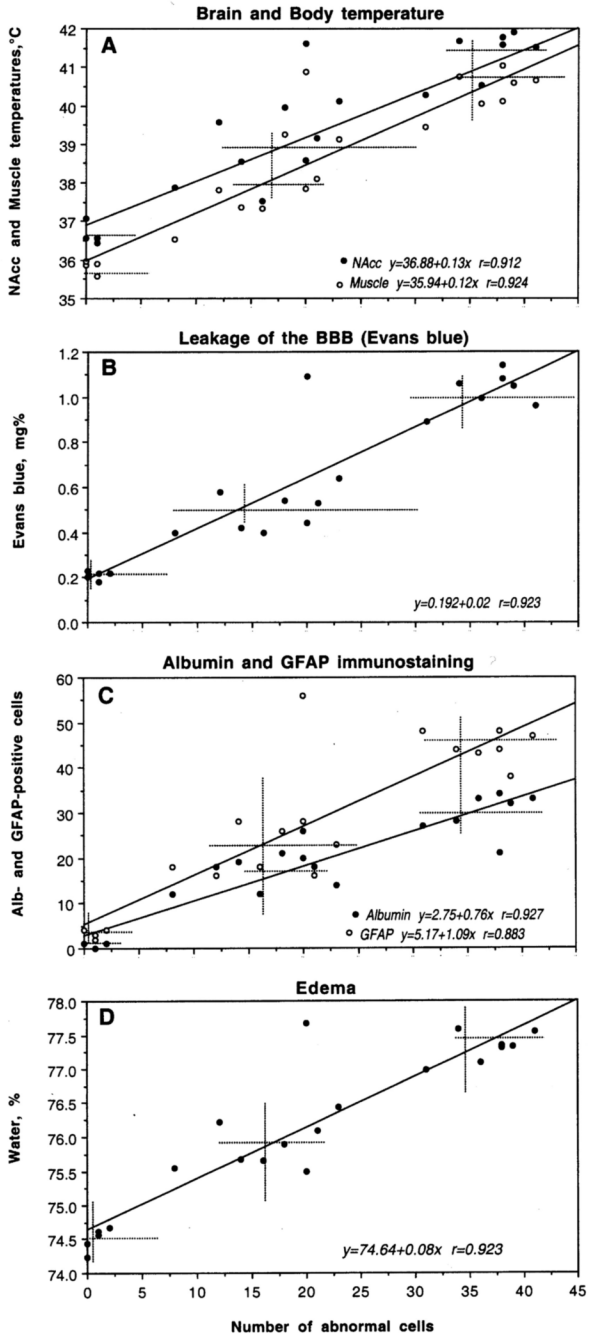

Fig. 7.

The relationships between cortical neural damage and several other functional parameters during acute METH intoxication. Abscissas in each graph shows the number of damaged cells encountered in cortex and ordinates show, respectively, NAcc and muscle temperatures (A), concentrations of Evans blue (B), the numbers of Albumin- and GFAP-positive neurons (C) and tissue water content (D). Each graph shows a regression line (s), regression equation (s), and coefficient(s) of correlation (r). Hatched lines show mean values.

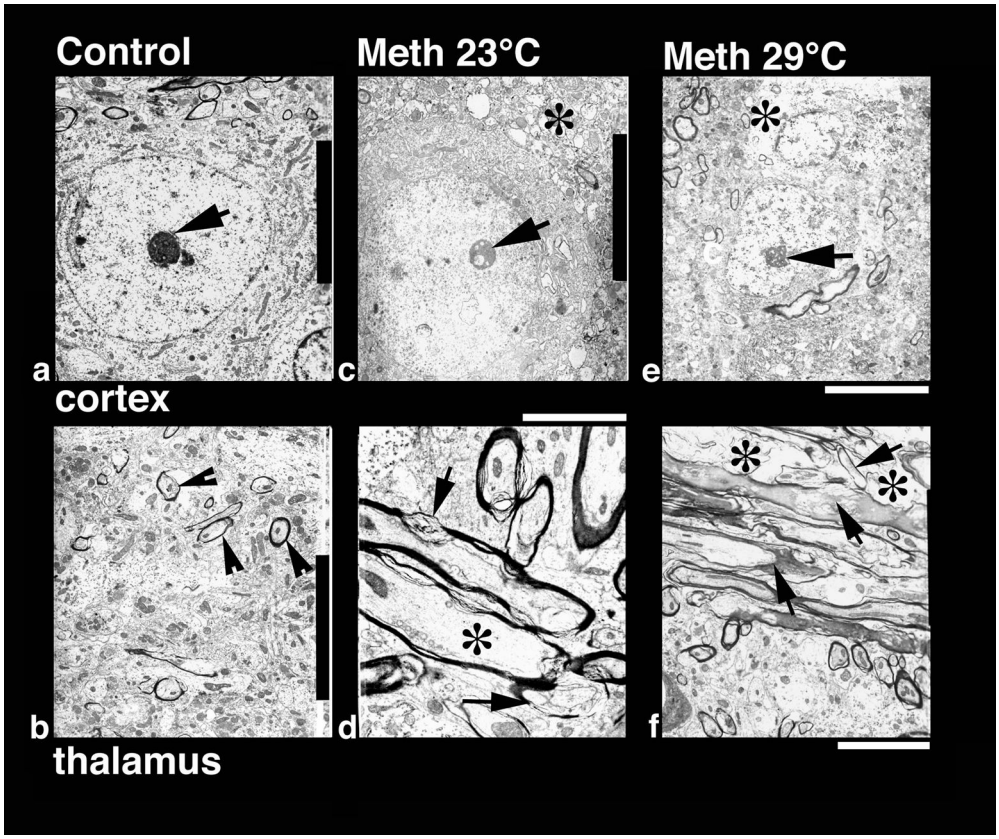

Fig. 8.

Low-power transmission electron micrograph from the cortex (upper panel) and thalamus (lower panel) showing neuronal nuclear (a, c, e) and axonal changes (b, d, f) in control (a, b), METH-23° C (c, d) and METH-29° C (e, f) groups. The neuronal nucleus in control rat shows a smooth nuclear envelope with a dark granular karyoplasm containing a central nucleolus (a, arrow). The nerve cell cytoplasm is compact and condensed without any vacuoles. On the other hand, a less electron-dense karyoplasm with an eccentric nucleolus showing degenerative changes is seen in the METH-23°C group (c, arrow). The nuclear membrane showed irregular foldings and vacuolation (*) in the neuropil including cytoplasm. These changes in the cell nucleus were much more aggravated in rats treated with METH at 29°C (e); degeneration of the nuclear membrane and surrounding neurnal cytoplasm is clearly evident in this slice. The nucleolus was further degenerated (arrow) and became more eccentric (e). Bar: a–c = 1 μm. Axonal changes in the thalamus of METH-treated rats at 23°C (d) show profound myelin vesiculation (arrow) and edematous swelling (*, d). These changes were stronger in rats treated with METH at 29° C (f). In this group, the myelin vesiculation (arrows) and degeneration of axons were clearly evident (*, f). On the other hand, normal rats exhibited a compact neuropil with normal myelinated axons (arrow heads, b). Signs of vacuolation and edema are largely absent in control group (a, b). Bars: b = 1500 nm, d = 800 nm; f = 600 nm.

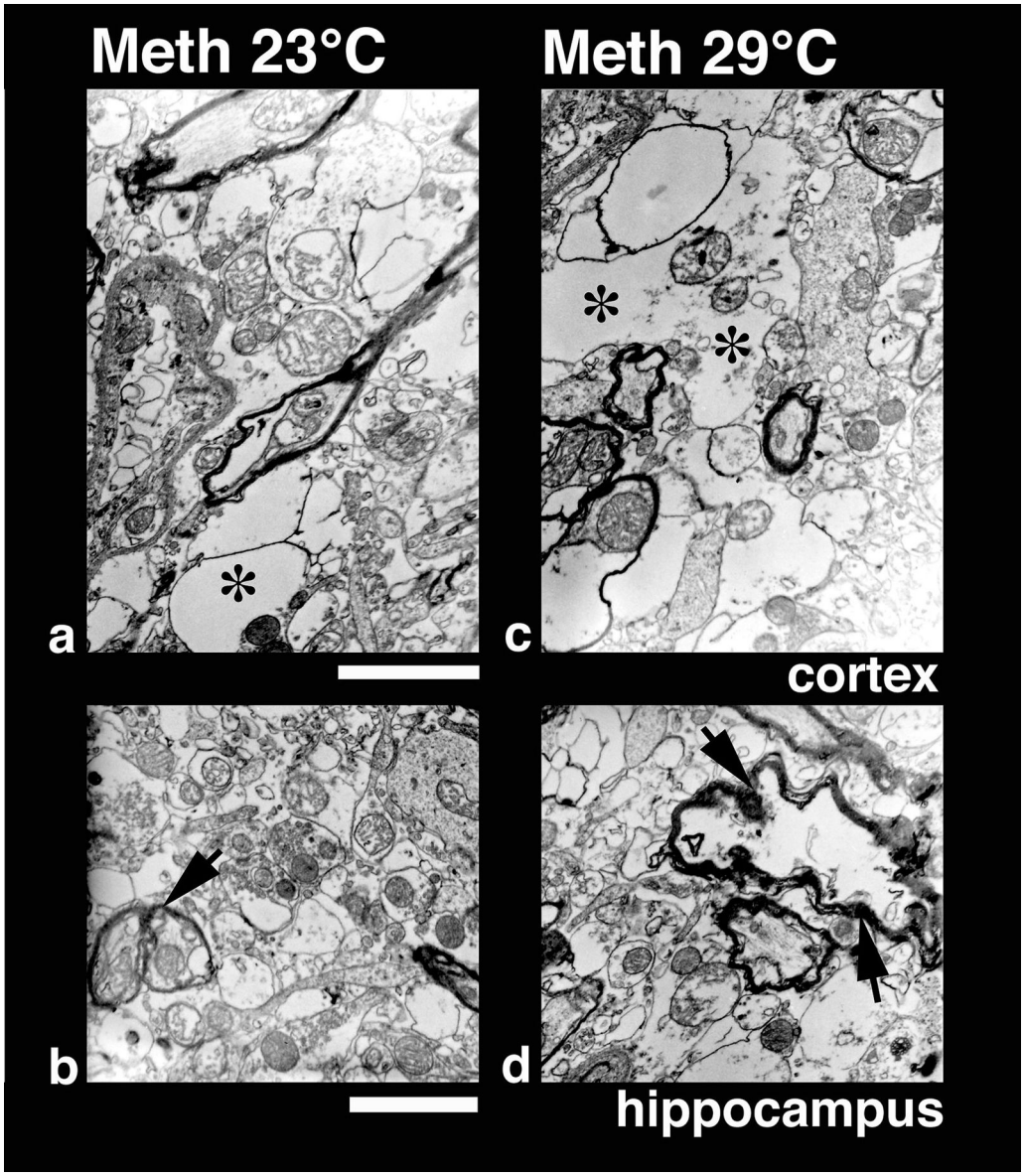

Fig. 9.

High-power transmission electron micrograph of neuropil from the cortex (upper panel) and hippocampus (lower panel) in rats treated with METH at 23° C (a, b) and 29° C (c, d). Vacuolation, edema (*) and degeneration of myelin are much more extensive and widespread in both the cortex (c) and hippocampus (d) in rats treated with METH at 29°C compared to 23°C (a, b). However, mitochondria in the neuropil are largely preserved showing normal cristae indicating that these membrane disruption and vacuolation are not due to fixation artifacts (for details see text). Bar: a, c = 600 nm; c, d = 800 nm.

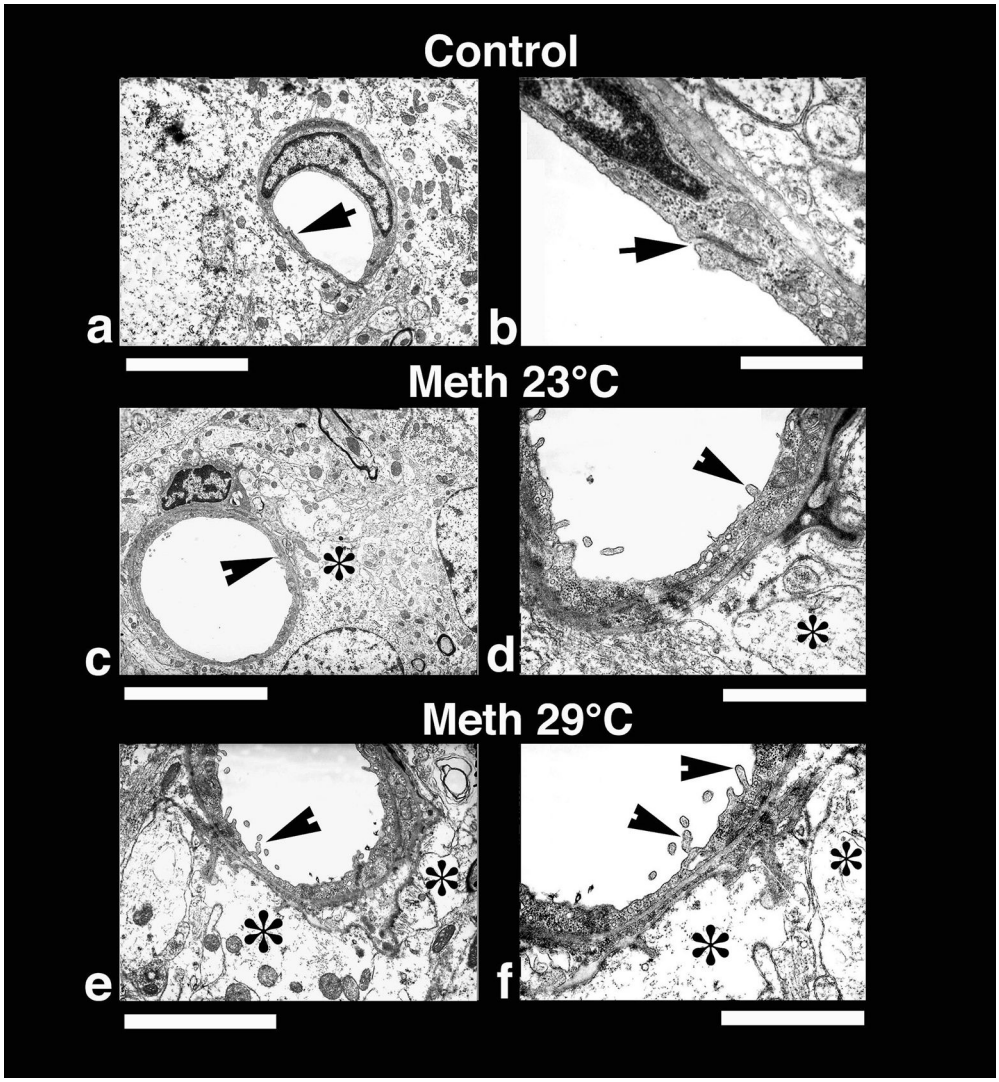

Fig. 10.

Low-power (left panel) and High-power (right panel) transmission electronmicrographs (left panel) showing a cerebral capillary and the surrounding neuropil in control (a and b) and METH-treated brain (c and d, 23°; e and f 29° C). A normal cerebral capillary has a smooth luminal surface and a compact, dense neuropil surrounding it and normal tight junctions (a, arrow). The normal capillary also has distinct tight junctions (b, arrow) and the underlying glial cells (astrocyte) do not exhibit any apparent signs of perivascular edema (b). METH treatment at 23°C resulted in endothelial cell reaction and swelling of the perivascular astrocyte (*, c). The endothelial luminal surface exhibited few distinct bleb formations (arrow head) indicating the process of enhanced vesicular transport or alterations in membrane transport properties (d, for details see text). Swollen perivascular astrocytes and its processes (*) are evident in this METH-treated rat (d). These ultratstructural changes, e.g., bleb formation and perivascular edema, were much more aggravated in the rat after METH treatment at 29°C (e, f). Thus, spreading out of small membrane vesicles and elongated bleb formation could be seen in this group (arrow heads). Swelling of astrocytes (*) and disintegration of astrocytic cytoplasm indicating water filled cells are clearly visible (*, f). The endothelial cell cytoplasm in METH-treated rats is much more condensed (d, f) compared to control (a, b). Bars: a, c = 1 μm, e = 2 μm,; b = 500 nm; d = 800 nm; f = 600 nm.

Table 1

Various brain parameters in rats exposed to METH at 23 and 29°C ambient temperatures

Parameters	Animal group		
	Control n=5	**METH-23° n=8C**	**METH-29°C n=8**
Evans Blue (mg %)			
Cortex	0.21±0.01	0.49±0.03***	1.03±0.03***,ooo
Hippocampus	0.26±0.01	0.61±0.02***	0.94±0.02***,ooo
Thalamus	0.39±0.01	0.65±0.01***	0.81±0.02***,ooo
Hypothalamus	0.42±0.01	0.72±0.02***	0.88±0.02***,ooo
Water content (%)			
Cortex	74.50±0.08	75.88±0.12***	77.35±0.09***,ooo
Hippocampus	78.39±0.05	79.75±0.15***	81.44±0.07***,ooo
Thalamus	75.50±0.06	76.81±0.19***	78.34±0.10***,ooo
Hypothalamus	75.45±0.08	76.32±0.15***	78.09±0.05***,ooo
Na^+ (mM/kg, dry wt.)			
Cortex	321.00±2.10	351.13±4.68***	376.75±3.55***,ooo
Hippocampus	348.00±2.83	384.00±6.07***	388.88±2.94***
Thalamus	305.60±2.50	338.00±3.76***	367.75±2.83***,ooo
Hypothalamus	307.80±1.56	343.75±6.91***	380.00±1.04***,ooo
K^+ (mM/kg, dry wt.)			
Cortex	221.20±2.15	212.13±2.55*	250.63±3.87***,ooo
Hippocampus	234.20±2.20	234.63±8.32	277.88±3.07***,ooo
Thalamus	210.00±0.89	243.50±6.70***	276.75±3.02***,ooo
Hypothalamus	208.20±1.43	226.25±5.70**	250.25±2.64***,ooo
Cl^- (mM/kg, dry wt.)			
Cortex	152.40±2.32	161.63±2.54*	171.00±3.38***,o
Hippocampus	164.40±1.50	158.75±3.16	174.38±1.66***,ooo
Thalamus	130.80±1.02	145.25±3.40***	162.88±1.23***,ooo
Hypothalamus	129.00±1.95	130.88±2.50	162.50±1.39***,ooo

Each value represents mean±sem.

Asterisks show values in the METH-23°C that are significantly different from control values (*, p <0.05; **, p <0.01;***, p < 0.001; Student's t-test).

Circles define differences between two METH groups (o, p<0.05; oo, p<0.01; ooo, p<0.001; Student's t-test).

Table 2

Neuropathological changes in rats exposed to METH at 23 and 29°C ambient temperatures

Parameters	Animal group		
	Control n=5	METH-23°C n=8	METH-29°C n=8
Damaged Neurons (cells/section)			
Cortex	0.80±0.38	16.50±1.77***	34.625±2.360***,ooo
Hippocampus	0.40±0.25	20.88±1.82***	31.625±1.890***,ooo
Thalamus	1.00±0.32	19.63±1.43***	29.625±1.917***,ooo
Hypothalamus	0.60±0.25	18.00±1.30***	27.500±1.402***,ooo
Albumin (+ cells/section)			
Cortex	0.60±0.25	16.75±1.26***	29.25±1.60***,ooo
Hippocampus	0.60±0.26	19.13±1.03***	26.88±1.49***,ooo
Thalamus	0.80±0.37	12.50±1.18***	17.88±1.13***,ooo
Hypothalamus	0.20±0.20	9.50±1.00***	15.00±0.78***,ooo
GFAP (+cells/section)			
Cortex	3.40±0.40	21.63±1.85***	46.00±1.84***,ooo
Hippocampus	6.20±0.80	25.13±1.06***	51.88±1.70***,ooo
Thalamus	3.60±0.68	27.25±1.24***	39.63±1.76***,ooo
Hypothalamus	2.00±0.32	16.38±1.46***	25.75±1.50***,ooo

Each value represents mean±sem.

Asterisks show values in the METH-23°C that are significantly different from control values (*, $p < 0.05$; **, $p < 0.01$;***, $p < 0.001$; Student's t-test).

Circles define differences between two METH groups (o, $p<0.05$; oo, $p<0.01$; ooo, $p<0.001$; Student's t-test).